Pharmaceutical Sciences, 2023, 29(2), 219-227
doi:10.34172/PS.2022.35
https://ps.tbzmed.ac.ir/

Research Article

Sensing of Letrozole Drug by Pure and Doped Boron Nitride Nanoclusters: Density Functional Theory Calculation

Afsoon Behmanesh[1], Farshid Salimi[1*], Gholamreza Ebrahimzadeh-Rajaei[1]

[1]*Department of Chemistry, Ardabil Branch, Islamic Azad University, Ardabil, Iran.*

Article Info

Article History:
Received: 11 Apr 2022
Accepted: 28 Jul 2022
ePublished: 29 Jul 2022

Keywords:
-Adsorption
-BN nanocluster
-Density functional theory
-Letrozole

Abstract

Background: Letrozole is a non-steroidal drug utilized as a treatment of hormone-sensitive breast cancer. It has been shown that letrozole has harmful side effects. Therefore, it seems necessary to design a letrozole drug sensor. In this work, we scrutinized the sensing properties of the $B_{30}N_{30}$, $AlB_{29}N_{30}$, and $GaB_{29}N_{30}$ nanoclusters toward the letrozole drug in various adsorption sites.

Methods: Investigations were done using the density functional theory (DFT) calculation with the B3PW91/6-311G(d, p) level of theory. The time-dependent density functional theory (TD-DFT) calculations were used to investigate Ultraviolet-visible (UV-vis) spectrums with the same level of theory.

Results: The adsorption energy of $B_{30}N_{30}$, $AlB_{29}N_{30}$, and $GaB_{29}N_{30}$ in the most stable complexes were calculated at -16.81, -34.62, and -27.41 kcal mol^{-1}, respectively. The results obtained from the study of electronic properties showed a high sensitivity for the detection of letrozole in $B_{30}N_{30}$ compared to $AlB_{29}N_{30}$ and $GaB_{29}N_{30}$. The calculated recovery time for the $B_{30}N_{30}$ is 0.13×10^{-5} s, which indicates a very short recovery time. The UV-vis spectrums showed that the letrozole/$B_{30}N_{30}$ exhibits shift toward the higher wavelengths (red shift).

Conclusion: Therefore, these results showed that the $B_{30}N_{30}$ is a good candidate for identifying letrozole. Further, $B_{30}N_{30}$ would be more effective than $AlB_{29}N_{30}$ and $GaB_{29}N_{30}$ due to the simple synthesis.

Introduction

Letrozole drug is a specific, potent, aromatase inhibitor, and non-steroidal currently used to treat hormone-sensitive breast cancer in postmenopausal women.[1-3] Due to various side effects such as headache, hot flashes, short half-life (≈ 45 h), and breast tenderness, it is essential to design a simple, rapid, and effective letrozole drug sensor.[4] Different techniques have been used for detecting letrozole, including chromatographic and spectrophotometric techniques.[5-8] These methods are generally time-consuming, more complicated, and expensive. Besides these costly and time-consuming techniques, it has been specified that nanomaterial-based chemical sensors can detect various materials at low concentrations because of the high volume/surface ratio.[9] The utilization of sensors has many advantages, such as easy construction against the easy analytical instrument, short reply time, low cost, and small size.

Nanostructures take advantage of high specific surface area, chemical activity, and enhanced diffusivity.[10-19] Various nanomaterials such as nanocone, nanowires, nanotubes, nanoclusters, and nanosheets have been widely utilized for chemical sensors.[20-26] For example, Sun *et al.*[27] studied the interaction of amantadine drug on the aluminum nitride (AlN) and boron nitride (BN) nanoclusters using density functional theory (DFT) calculations. Results indicated amantadine interacts via its $-NH_2$ region with the BN and AlN nanoclusters. The adsorption energies of BN and AlN nanoclusters were calculated at -1.36 and -1.67 eV, respectively. After the adsorption of amantadine in the BN nanocluster, the E_g (energy gap) decreased significantly and increased electrical conductivity. Thus, the results of E_g indicated BN nanocluster could be a potential sensor for sensing amantadine.

Among various nanostructures, BN nanoclusters as inorganic nanostructures have been developed due to their excellent chemical, physical, and electronic properties.[28-31] Xia *et al.*[32] have indicated that the $B_{30}N_{30}$ nanocluster would be relatively simple to synthesize and stable. $B_{30}N_{30}$ nanoclusters have attracted much attention among scientific and engineering communities for various applications.[33-36] Yin *et al.*[37] confirmed the thermodynamical and vibrational stability of $B_{30}N_{30}$ by the symmetric first-principles calculations.Furthermore, they calculated the total energy

*Corresponding Author: Farshid Salimi, E-mail: Salimi982020@gmail.com

of six, seven, and eight homogenous bond isomers (N-N and B-B bonds) of $B_{30}N_{30}$ and found that the $B_{30}N_{30}$ with 6 N-N (B-B) bonds is the most stable configuration compared to the 7 and 8 homogenous bonds. Therefore, the $B_{30}N_{30}$ nanocluster with 6 homogenous bonds was used in this study. Computational methods significantly help the experimentalist to understand different compounds' behavior.[38-42] In this study, the adsorption of letrozole on the $B_{30}N_{30}$ nanoclusters was investigated using DFT calculations. Furthermore, we inserted Al and Ga atom instead of B atom in the $B_{30}N_{30}$ ($AlB_{29}N_{30}$ and $GaB_{29}N_{30}$) to find a suitable sensor for the letrozole drug.

Methods

Adsorption of letrozole drug onto the $B_{30}N_{30}$, $AlB_{29}N_{30}$ and $GaB_{29}N_{30}$ nanoclusters surfaces was calculated using DFT and time-dependent density functional theory (TD-DFT). All calculations were carried out using the Gaussian 09 program package[43] with the B3PW91/6-311G(d, p) level of theory.[44,45] The previous studies were reported that the B3PW91 method is one of the better methods,[46,47] and 6-311G(d, p) basis set known convenient for nanocarrier systems.[48,49] The adsorption energies (E_{ad}) of letrozole onto the $B_{30}N_{30}$, $AlB_{29}N_{30}$ and $GaB_{29}N_{30}$ nanoclusters were obtained with the following equations:

$$E_{ad} = E\ (Letrozole/B_{30}N_{30}) - E\ (B_{30}N_{30}) - E\ (Letrozole) \quad \textbf{Eq. (1)}$$

$$E_{ad} = E\ (Letrozole/AlB_{29}N_{30}) - E\ (AlB_{29}N_{30}) - E\ (Letrozole) \quad \textbf{Eq. (2)}$$

$$E_{ad} = E\ (Letrozole/GaB_{29}N_{30}) - E\ (GaB_{29}N_{30}) - E\ (Letrozole) \quad \textbf{Eq. (3)}$$

where E ($Letrozole/B_{30}N_{30}$), E ($Letrozole/AlB_{29}N_{30}$), and E ($Letrozole/GaB_{29}N_{30}$) are the total energies of the $B_{30}N_{30}$, $AlB_{29}N_{30}$ and $GaB_{29}N_{30}$ interacted with letrozole. E (Letrozole), E ($B_{30}N_{30}$), E ($AlB_{29}N_{30}$), and E ($GaB_{29}N_{30}$) are the total energy of the lone letrozole, $B_{30}N_{30}$, $AlB_{29}N_{30}$ and $GaB_{29}N_{30}$, respectively. Thermodynamic parameters (enthalpy (ΔH), entropy (ΔS), and Gibbs free energy (ΔG)) were also investigated at the same method to check the validity of the optimization. Furthermore, the density of states (DOS), molecular electrostatic potential (MEP), natural bond orbital (NBO), and all energy calculations analyses were investigated.

Results and Discussion

Adsorption of letrozole onto the $B_{30}N_{30}$

The letrozole optimized structure and MEP plot are indicated in Figure 1. The MEP plot shows that the negative charges are mainly localized on the 25 Nitrogen (N), 26N, 32N, and 33N atoms (yellow and red), which can be adsorbed on the electron-withdrawing parts of the nanoclusters.

First, the structure of the $B_{30}N_{30}$ nanocluster was optimized, and the most stable structure was reported in Figure 2. Then, the interaction of letrozole with $B_{30}N_{30}$ was investigated in diverse adsorption sites (Figure 2). The E_{ad} of letrozole with the $B_{30}N_{30}$ in states A, B, C, and D was investigated about -4.60, -5.60, -11.43, and -16.81 kcal mol^{-1} with equilibrium distances of 1.69, 1.69, 1.64, and 1.62 Å, respectively. Thus, the adsorption of the letrozole from its 33N with the $B_{30}N_{30}$ (state D) is the most stable adsorption site. Furthermore, using molecular dynamic simulation with the AMBER force field, the adsorption energies were calculated at -8.00, -7.99, -9.14, and -11.91 kcal mol^{-1} in states A, B, C, and D, respectively. Thus, similar to the DFT method, the molecular dynamic simulation indicated the adsorption from state D is the most stable. We calculated the E_{ad} of letrozole with the C_{60} nanocluster at 4.38 kcal mol^{-1}.[50] Therefore, the E_{ad} value indicated appropriate interaction in the $B_{30}N_{30}$ nanocluster compared with the C_{60} nanocluster. The Mulliken charge transfers from the letrozole to the $B_{30}N_{30}$ in states A, B, C, and D were investigated at about 0.279, 0.288, 0.219, and 0.264 e, respectively. Furthermore, the natural bond orbital (NBO) charge transfers were calculated at 0.302, 0.307, 0.322, and 0.337 e. Positive values of NBO charge transfers illustrated that the charge transferred from letrozole to $B_{30}N_{30}$ nanocluster. The dipole

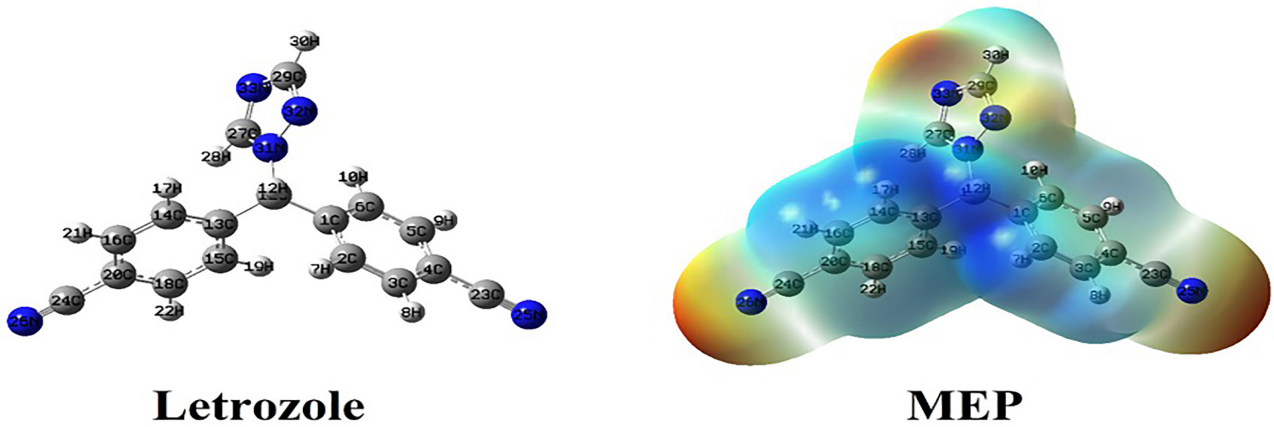

Figure 1. optimized structure and MEP plots of the letrozole drug. (The color scheme for MEP surface is red-electron rich or partially negative charge; blue-electron deficient or partially positive charge; light blue-slightly electron deficient region; yellow-slightly electron rich region, respectively).

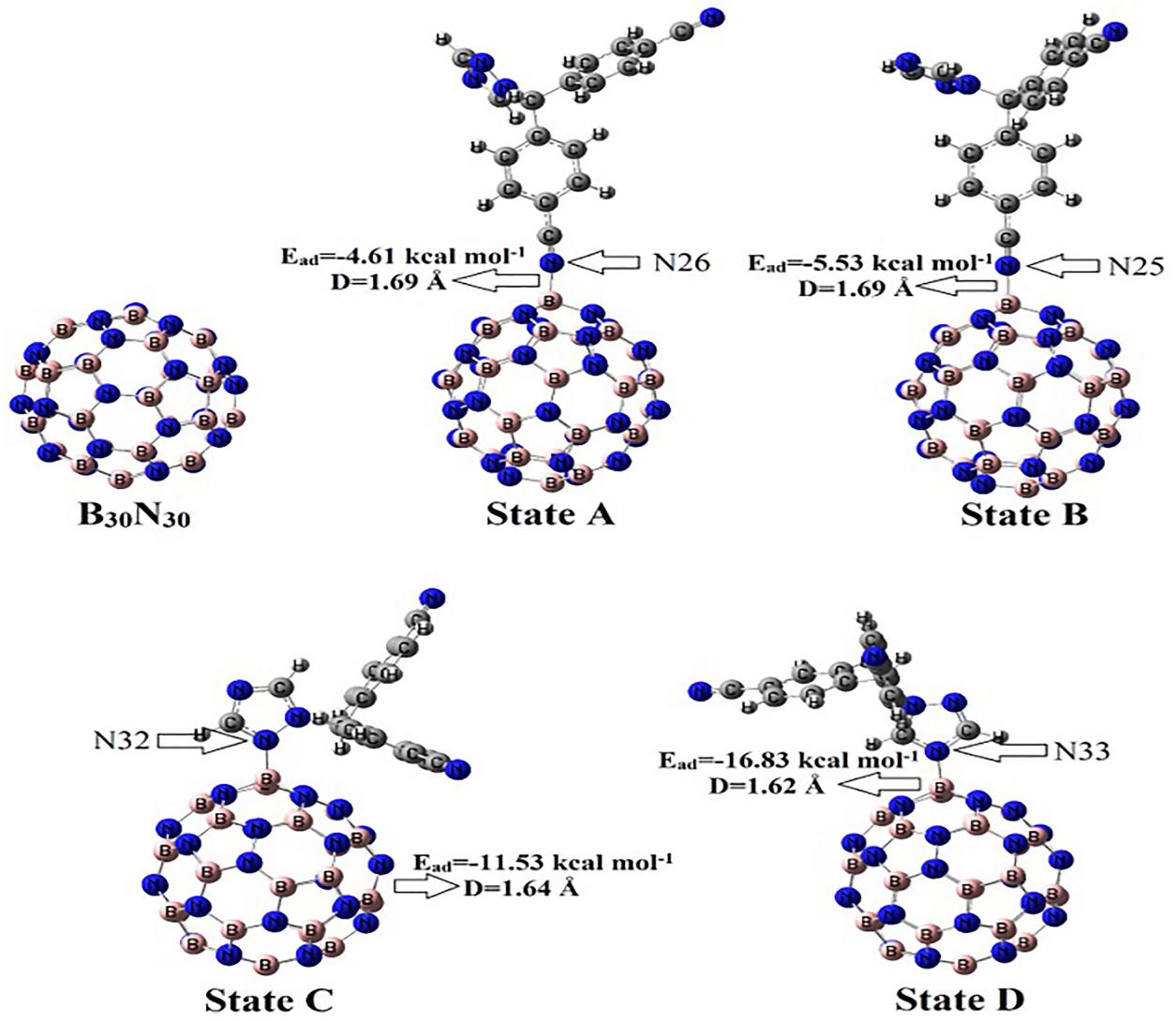

Figure 2. Optimized structure for the pure $B_{30}N_{30}$ and $B_{30}N_{30}$/letrozole complexes in state A, B, C and D.

moment (DM) value in pure $B_{30}N_{30}$ was increased from 0.14 Debye to 8.47, 10.18, 6.85, and 8.66 Debye in states A, B, C, and D, respectively, which make them more soluble in polar solvents after adsorption. The ΔH values for the $B_{30}N_{30}$ nanocluster were investigated at -2.30, -2.96, -8.13, and -14.51 kcal mol^{-1}, and the ΔG values were calculated at about -0.16, -0.83, 6.23, and -11.12 kcal mol^{-1} in state A, B, C, and D, respectively. Thus, these results approved that the adsorption of letrozole in state D is stronger since ΔH and E_{ad} values indicated in state D are more negative than that of other states.

Adsorption of letrozole onto the AlB29N30 and GaB29N30

In the following, the Boron (B) atom of the $B_{30}N_{30}$ nanocluster was altered with Aluminum (Al) or Gallium (Ga) atom ($AlB_{29}N_{30}$ and $GaB_{29}N_{30}$) for adsorption of letrozole. The most stable structures of letrozole/$AlB_{29}N_{30}$ and letrozole/$GaB_{29}N_{30}$ complexes in the different states are shown in Figures 3 and 4. The E_{ad} of letrozole/$AlB_{29}N_{30}$ in states E, F, G, and H was calculated to be -24.40, -25.41, -28.88, and -34.62 kcal mol^{-1}, respectively (Table 1). The equilibrium distance of letrozole and $AlB_{29}N_{30}$ nanocluster was determined 1.99, 1.99, 2.00, and 1.98 Å, and NBO (Mulliken) charge transfer was calculated to be 0.153 (0.173), 0.171 (0.179), 0.183 (0.130), and 0.182 (0.169) e in state E, F, G, and H, respectively. Therefore, charge transfer from drug to nanoclusters. The ΔH values for the $AlB_{29}N_{30}$ nanocluster are calculated at -23.18, -23.98, -26.32, and -31.56 kcal mol^{-1} in states E, F, G, and H, respectively. The ΔG values in states E, F, G, and H are calculated at -19.63, -20.22, -21.57, and -28.02 kcal mol^{-1}, respectively. The E_{ad} of letrozole/$GaB_{29}N_{30}$ in the state I, J, K, and L was calculated to be -17.59, -18.45, -22.98, and -27.41 kcal mol^{-1} with equilibrium distances of 2.04, 2.04, 2.05, and 2.03 Å, respectively. Similar to the $B_{30}N_{30}$ and $AlB_{29}N_{30}$ nanoclusters, the NBO and Mulliken charge transfers for letrozole/$GaB_{29}N_{30}$ complexes demonstrated a charge transfer from letrozole to $GaB_{29}N_{30}$ nanocluster. These results indicated that the adsorption of the $AlB_{29}N_{30}$ nanocluster is stronger than $B_{30}N_{30}$ and $GaB_{29}N_{30}$ nanoclusters. Similar to the $B_{30}N_{30}$, the adsorption of the letrozole from its 33N

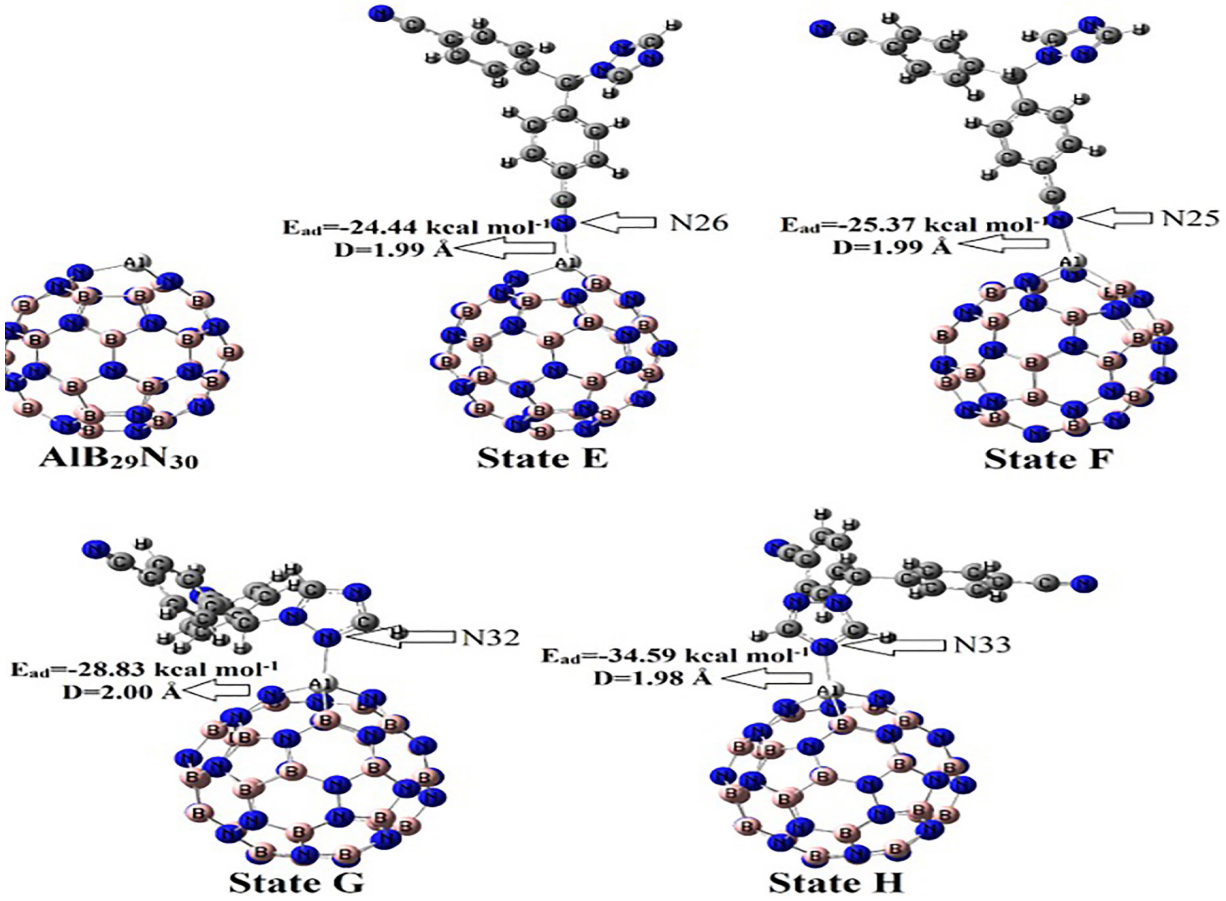

Figure 3. Optimized structure for the pure $AlB_{29}N_{30}$ and $AlB_{29}N_{30}$/letrozole complexes in state E, F, G and H.

with $AlB_{29}N_{30}$ and $GaB_{29}N_{30}$ nanoclusters (states H and L) are the most stable. The DM values were enhanced after the letrozole interaction with nanoclusters. These results indicate an increase in solubility after letrozole adsorption on the nanoclusters. Thus, negative values indicated that the interaction of letrozole with the $B_{30}N_{30}$, $AlB_{29}N_{30}$, and $GaB_{29}N_{30}$ is exothermic, and the letrozole's adsorption is spontaneous. The E_{ad} calculated values are more negative than the ΔG values, indicating ΔS reduction (Table 1).

Table 1. Calculated adsorption energy (E_{ad}/kcal mol^{-1}), bond distance between letrozole and nanocluster (D/Å), Charge on the letrozole in complexes (Q/e), HOMO energies ($E_{(HOMO)}$/eV), LUMO energies ($E_{(LUMO)}$/eV), energy gap (Eg/eV), change of Eg after adsorption (%ΔEg/% and dipole moment (DM/Debye).

Name	E_{ad}	D	Q	$E_{(HOMO)}$	$E_{(LUMO)}$	E_g	%ΔE_g	DM	ΔH	ΔG	ΔS
Letrozole	-	-	-	-7.74	-2.43	5.32	-	2.66	-	-	
$B_{30}N_{30}$	-	-	-	-6.72	-2.09	4.63	-	0.14	-	-	
A	-4.60	1.69	0.279	-5.79	-3.33	2.45	-47.08	8.47	-2.30	-0.16	-0.007
B	-5.60	1.69	0.288	-5.74	-3.15	2.59	-44.06	10.18	-2.96	-0.83	-0.007
C	-11.43	1.64	0.219	-6.13	-2.68	3.45	-25.49	6.85	-8.13	-6.23	-0.006
D	-16.81	1.62	0.264	-5.86	-2.86	3.00	-35.21	8.66	-14.51	-11.12	-0.011
$AlB_{29}N_{30}$	-	-	-	-6.47	-2.65	3.83	-	2.64	-	-	
E	-24.40	1.99	0.173	-5.61	-3.8	1.80	-53.00	13.11	-23.18	-19.63	-0.012
F	-25.41	1.99	-0.179	-5.56	-3.63	1.93	-49.61	14.80	-23.98	-20.22	-0.013
G	-28.88	2.00	0.130	-6.00	-2.83	3.17	-17.23	7.22	-26.32	-21.57	-0.016
H	-34.62	1.98	0.169	-5.74	-2.95	2.79	-27.15	12.14	-31.56	-28.02	-0.012
$GaB_{29}N_{30}$	-	-	-	-6.48	-2.88	3.60	-	2.21	-	-	-
I	-17.59	2.04	0.136	-5.61	-3.64	1.97	-45.28	12.06	-15.22	-11.46	-0.013
J	-18.45	2.04	0.142	-5.56	-3.46	2.10	-41.67	13.83	-16.41	-13.69	-0.009
K	-22.98	2.05	0.108	-5.95	-2.81	3.14	-12.78	6.83	-21.03	-17.37	-0.012
L	-27.41	2.03	0.176	-5.71	-2.88	2.83	-21.39	11.10	-25.18	-22.94	-0.011

The MEP plots of pure and complexes of nanoclusters are indicated in Figure 5. The electrostatic potential in Al and Ga atoms of $AlB_{29}N_{30}$ and $GaB_{29}N_{30}$ compared to the $B_{30}N_{30}$ is significantly more positive (blue color), making it the most electron-withdrawing site for N atoms of the molecule. Adsorption of letrozole on $B_{30}N_{30}$, $AlB_{29}N_{30}$, and $GaB_{29}N_{30}$ in states D, H, and L significantly changed their MEP plots. The MEP maps after the adsorption process indicated that the letrozole drug is more positive (blue color). These results showed charge transfers from the letrozole drug to nanoclusters and confirmed the results of NBO charge transfers.

Evaluation of the electrical properties of letrozole on the nanoclusters

The electronic properties of $B_{30}N_{30}$, $AlB_{29}N_{30}$, and $GaB_{29}N_{30}$ nanoclusters before and after adsorption of the letrozole drug are indicated in Table 1. In the $B_{30}N_{30}$ nanocluster, the HOMO and LUMO energies are about -6.72 and -2.09 eV, respectively. Therefore, the E_g was calculated at 4.63 eV. The electronic properties significantly changed in the $AlB_{29}N_{30}$ and $GaB_{29}N_{30}$ nanoclusters. The HOMO and LUMO energies for $AlB_{29}N_{30}$ were calculated at -6.47 and -2.65 eV, respectively. Also, the HOMO and LUMO values of $GaB_{29}N_{30}$ were calculated at -6.48 and -2.28 eV, respectively. These results demonstrated that inserting the Ga or Al atoms instead of the B atom destabilizes the HOMO and stabilizes the LUMO levels. Therefore, in the $AlB_{29}N_{30}$ and $GaB_{29}N_{30}$ nanoclusters, the E_g values were reduced by 17.28% and 22.25% compared with the $B_{30}N_{30}$ nanocluster. After adsorption of letrozole, in the most stable complex of the letrozole/$B_{30}N_{30}$ (state D), the LUMO level is stabilized by shifting from -2.09 to -2.86 eV, and the HOMO level is destabilized by about 0.86 eV. These changes in the LUMO and HOMO levels significantly decreased the E_g of the $B_{30}N_{30}$ from 4.63 to 3.00 eV (-35%). In the most stable letrozole/$AlB_{29}N_{30}$ and letrozole/$GaB_{29}N_{30}$ complexes (states H and L), the E_g changed about -27.15% and -21.39%. The E_g values show reactivity and sensitivity. The lower values indicate higher sensitivity, reactivity, and electrical conductivity since the change in E_g values corresponds to the population of conduction elections, as stated in Eq. 4.[51]

$$A = AT^{3/2} exp\left(\frac{-E\,g}{2KT}\right) \qquad \textbf{Eq.(4)}$$

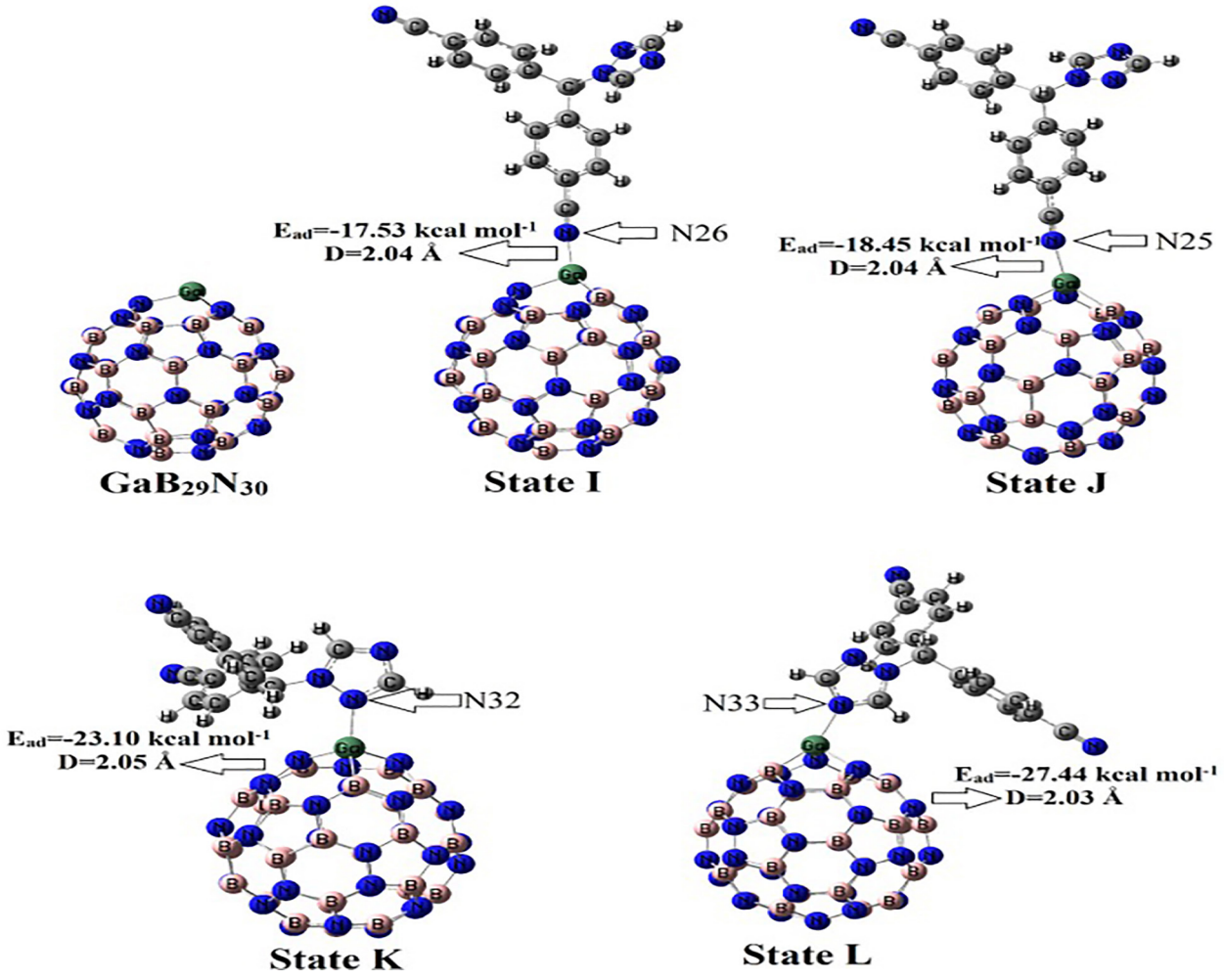

Figure 4. Optimized structure for the pure $GaB_{29}N_{30}$ and $GaB_{29}N_{30}$/letrozole complexes in state I, J, K and L.

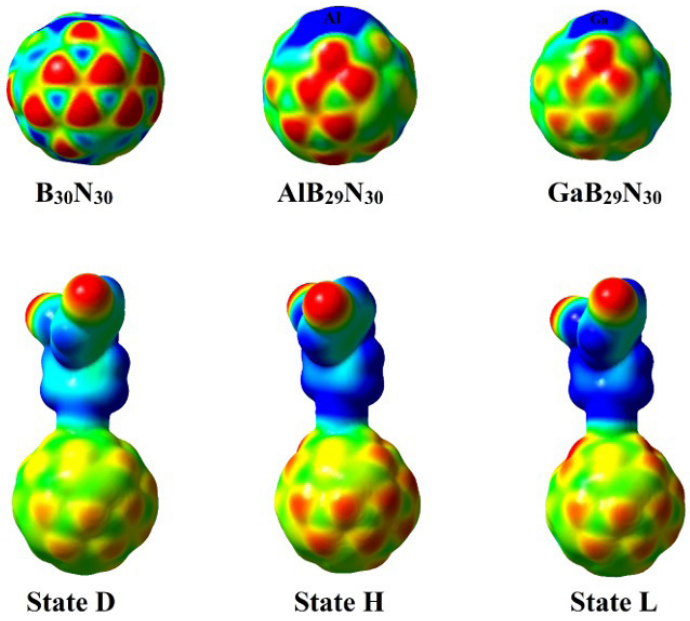

Figure 5. MEP plots of pure $B_{30}N_{30}$, $AlB_{29}N_{30}$ and $GaB_{29}N_{30}$ nanoclusters and letrozole/$B_{30}N_{30}$ (state D), letrozole/$AlB_{29}N_{30}$ (state H) and letrozole/$GaB_{29}N_{30}$ (state L).

Where A, K, and T are a constant in electrons/$m^3.K^{3/2}$, Boltzmann's constant, and temperature, respectively. Bearing in mind Eq. (4), the population of electrical conductivity increases exponentially as E_g decreases, which is changed into an electrical signal. Thus, it is clear that the letrozole/$B_{30}N_{30}$ is more sensitive rather than letrozole/$AlB_{29}N_{30}$ and letrozole/$GaB_{29}N_{30}$. Decrease the E_g through adsorption of letrozole shown the $B_{30}N_{30}$ could detect the letrozole. The DOS plot in Figure 6 corroborated that this alteration in the E_g region of $B_{30}N_{30}$ is more pronounced than $AlB_{29}N_{30}$ and $GaB_{29}N_{30}$ nanoclusters.

Recovery time

The kind of recovery time and interaction is significant for sensor development. Since strong interactions often cause long recovery times, which are not ideal for sensor applications. The recovery time is recognized experimentally by exposure to UV light or heating the adsorbent to higher temperatures.[52] Thus, the recovery time of $B_{30}N_{30}$, $AlB_{29}N_{30}$, and $GaB_{29}N_{30}$ nanoclusters was calculated with the following equations:

$$\tau = \upsilon_0^{-1} exp\left(-\Delta G / kT\right) \qquad \text{Eq. (5)}$$

where T, k, and ν_0 are the temperature, Boltzmann's constant, and attempt frequency, respectively. If UV of 10^{14} s^{-1} ($\nu \sim 10^{14}$ s^{-1}) is used for attempt frequency to extract the letrozole attached to the nanoclusters, the recovery time for the letrozole/$B_{30}N_{30}$, letrozole/$AlB_{29}N_{30}$, and letrozole/$GaB_{29}N_{30}$ will be about 0.13×10^{-5}, 33.13×10^{5}, and 709.95 s at ambient temperature, respectively. These results showed that the $AlB_{29}N_{30}$ and $GaB_{29}N_{30}$ suffer from a long recovery time and could not be practical as a letrozole drug sensor. Also, the $B_{30}N_{30}$ has a suitable short recovery time. Thus,

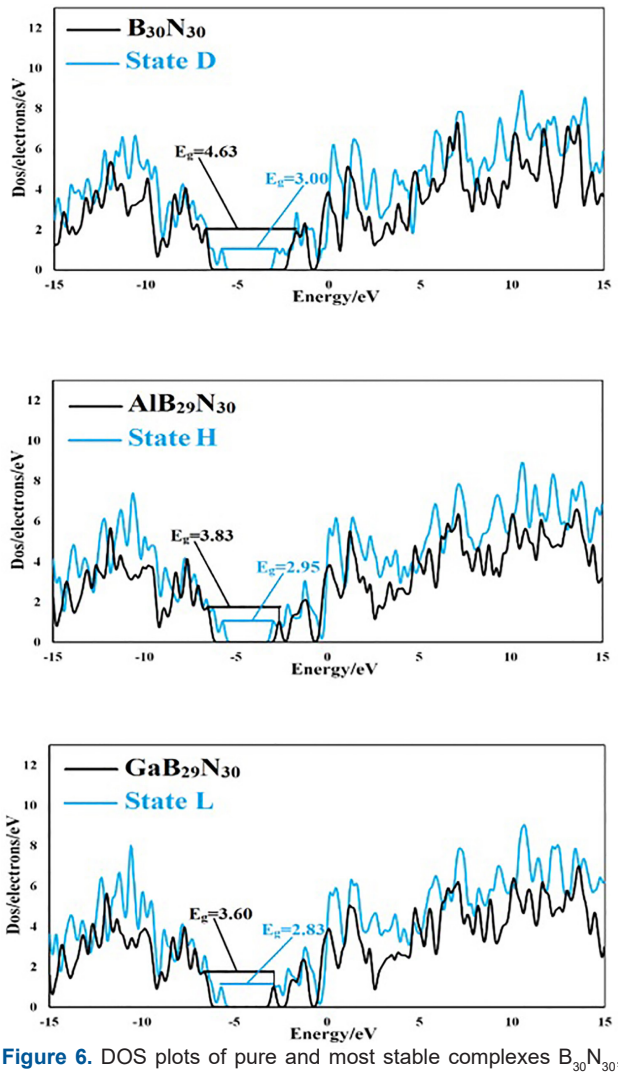

Figure 6. DOS plots of pure and most stable complexes $B_{30}N_{30}$, $AlB_{29}N_{30}$ and $GaB_{29}N_{30}$ nanoclusters.

the $B_{30}N_{30}$ nanocluster is an appropriate candidate for sensing the letrozole drug.

Ultraviolet–visible (UV–vis) spectra

The TD-DFT calculations were utilized to investigate UV-vis spectrums of pure nanoclusters and the most stable complexes. In Table 2, the highest oscillator strengths (f) for the current study nanoclusters were shown. The λ_{max} has existed in the spectra of $B_{30}N_{30}$, $AlB_{29}N_{30}$, and $GaB_{29}N_{30}$ nanoclusters placed at 306, 398, and 427 nm, respectively. After the adsorption of letrozole on the nanoclusters, λ_{max} of complexes shifted to a higher wavelength (red shift). The maximum λ_{max} shift was related to the letrozole/$B_{30}N_{30}$ (162 nm). The UV-vis spectrum of $B_{30}N_{30}$ and letrozole/$B_{30}N_{30}$ was shown in Figure 7.

Conclusion

In this work, the adsorption of letrozole drug on the $B_{30}N_{30}$, $AlB_{29}N_{30}$, and $GaB_{29}N_{30}$ nanoclusters was investigated using DFT calculations to find a new system for the detection of letrozole drug. The calculations of E_{ad} indicated favorable interaction between letrozole and $B_{30}N_{30}$ nanocluster. We found that the adsorption of letrozole with $AlB_{29}N_{30}$ and $GaB_{29}N_{30}$ is greater, which can increase its recovery time. The E_g values and DOS plots indicated that the $B_{30}N_{30}$ has greater sensitivity to the letrozole than the $AlB_{29}N_{30}$ and $GaB_{29}N_{30}$. Thus, our findings determined that the $B_{30}N_{30}$ nanocluster can selectively identify the letrozole drug.

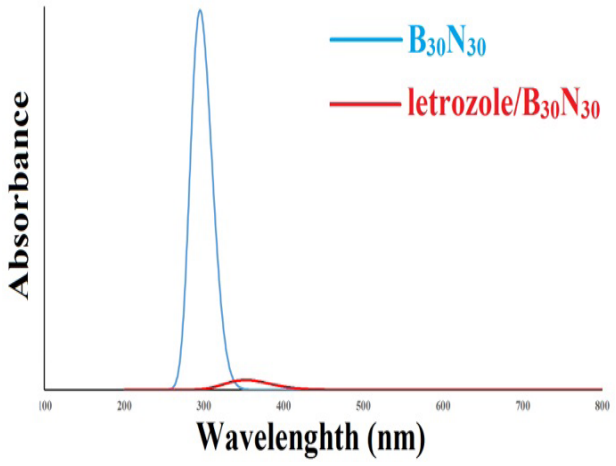

Figure 7. The UV-vis spectrum of $B_{30}N_{30}$ and letrozole/$B_{30}N_{30}$.

Author Contributions

AB: the acquisition, interpretation of data for the work, and drafting the work. FS: interpretation of data for the work, drafting the work, and revising. GER: interpretation of data for the work, drafting the work, and revising. The final manuscript was read and approved by the authors.

Conflict of Interest

The authors report no conflicts of interest.

References

1. Mondal N, Pal TK, Ghosal SK. Development and validation of rp-hplc method to determine letrozole in different pharmaceutical formulations and its application to studies of drug release from nanoparticles. Acta Pol Pharm Drug Res. 2009;66(1):11-7.
2. Dange Y, Bhinge S, Salunkhe V. Optimization and validation of rp-hplc method for simultaneous estimation of palbociclib and letrozole. Toxicol Mechan Methods. 2018;28(3):187-94. doi:10.1080/15376516.2017.1388458
3. Kil KE, Biegon A, Ding YS, Fischer A, Ferrieri RA, Kim SW, et al. Synthesis and pet studies of [11c-cyano] letrozole (femara), an aromatase inhibitor drug. Nucl Med Biol. 2009;36(2):215-23. doi:10.1016/j.nucmedbio.2008.11.010
4. Nabieva N, Fehm T, Häberle L, de Waal J, Rezai M, Baier B, et al. Influence of side-effects on early therapy persistence with letrozole in post-menopausal patients with early breast cancer: Results of the prospective evaluate-TM study. Eur J Cancer. 2018;96:82-90. doi:10.1016/j.ejca.2018.03.020
5. Farthing CA, Farthing DE, Koka S, Larus T, Fakhry I, Xi L, et al. A simple and sensitive hplc fluorescence method for determination of tadalafil in mouse plasma. J Chromatogr B Anal Technol Biomed Life Sci. 2010;878(28):2891-5. doi:10.1016/j.jchromb.2010.07.022
6. RodríguezJ,CastañedaG,MuñozL.Rapiddetermination of letrozole, citalopram and their metabolites by high performance liquid chromatography-fluorescence detection in urine: Method validation and application to real samples. J Chromatogr B Anal Technol Biomed Life Sci. 2013;913-914:12-8. doi:10.1016/j.jchromb.2012.11.015
7. Annapurna MM, Mohapatro C, Narendra A. Stability-

Table 2. Calculated maximum absorption wavelength (λ), oscillator strengths (f), and dominant transition contribution for the studied systems.

Molecule	λ_{max} (nm)	*f*	Major contribution
B30N30	306	0.0141	HOMOLUMO (68%), H-1LUMO (28%)
D	468	0.0013	HOMO®
$AlB_{29}N_{30}$	398	0.0382	HOMOLUMO (92%), H-2LUMO (5%)
H	508	0.0005	HOMOLUMO (100%),
$GaB_{29}N_{30}$	427	0.0347	HOMO®
L	509	0.0011	HOMOLUMO (99%)

indicating liquid chromatographic method for the determination of letrozole in pharmaceutical formulations. J Pharm Anal. 2012;2(4):298-305. doi:10.1016/j.jpha.2012.01.010
8. Acharjya SK, Mallick P, Panda P, Kumar KR, Annapurna MM. Spectrophotometric methods for the determination of letrozole in bulk and pharmaceutical dosage forms. J Adv Pharm Technol Res. 2010;1(3):348-53. doi:10.4103/0110-5558.72425
9. Foroughi MM, Ranjbar M. Graphene oxide doped with pbo nanoparticles, synthesis by microwave assistant thermal decomposition and investigation of optical property. J Cluster Sci. 2017;28(5):2847-56. doi:10.1007/s10876-017-1248-3
10. Moghaddam MD, Jamehbozorgi S, Rezvani M, Izadkhah V, Moghim MT. Theoretical treatment of interaction of pyrazinamide with graphene and h-sic monolayer: A DFT-D3 study. Phys E. 2022;138:115077. doi:10.1016/j.physe.2021.115077
11. Ganji MD, Nashtahosseini M, Yeganegi S, Rezvani M. First-principles vdw-df investigation on the interaction between the oxazepam molecule and c60 fullerene. J Mol Model. 2013;19(4):1929-36. doi:10.1007/s00894-013-1758-3
12. Rasoolidanesh M, Astaraki M, Mostafavi M, Rezvani M, Darvish Ganji M. Toward efficient enantioseparation of ibuprofen isomers using chiral bnnts: Dispersion corrected dft calculations and dftb molecular dynamic simulations. Diamond Relat Mat. 2021;119:108561. doi:10.1016/j.diamond.2021.108561
13. Rezvani M, Darvish Ganji M, Faghihnasiri M. Encapsulation of lamivudine into single walled carbon nanotubes: A vdW-DF study. Phys E. 2013;52:27-33. doi:10.1016/j.physe.2013.03.024
14. Rezvani M, Ahmadnezhad I, Darvish Ganji M, Fotukian MJJoN. Theoretical insights into the encapsulation of anticancer oxaliplatin drug into single walled carbon nanotubes. J Nanoanalysis. 2016;3(3):69-75. doi:10.22034/JNA.2016.03.001
15. Rezvani M, Astaraki M, Rahmanzadeh A, Darvish Ganji M. Theoretical assessments on the interaction between amino acids and the g-mg3n2monolayer: Dispersion corrected dft and dft-md simulations. Phys Chem Chem Phys. 2021;23(32):17440-52. doi:10.1039/d1cp02891j
16. Ganji MD, Rezvani M, Shokry M, Mirnejad A. First-principles investigation on the formation of endohedral complexes between CH4 molecules and Si60 fullerene nanocage. Fullerenes Nanotubes Carbon Nanostruct. 2011;19(5):421-8. doi:10.1080/1536383X.2010.481059
17. Ganji MD, Mousavy M, Rezvani M. On the encapsulation of azafullerenes inside the single-walled carbon nanotubes: Density-functional theory based treatments. Phys B Condens Matter. 2011;406(8):1561-6. doi:10.1016/j.physb.2011.01.070
18. Abbaspour-Gilandeh E, Aghaei-Hashjin M, Jahanshahi P, Hoseininezhad-Namin MS. One-pot synthesis of pyrano[3,2-c]quinoline-2,5-dione derivatives by Fe3O4@Sio2-SO3H as an efficient and reusable solid acid catalyst. Monatsh Chem. 2017;148(4):731-8. doi:10.1007/s00706-016-1788-5
19. Baniya HB, Guragain RP, Subedi DP. Cold atmospheric pressure plasma technology for modifying polymers to enhance adhesion: A critical review. Rev Adhes Adhes. 2021;9(2):269-307. doi:10.7569/RAA.2021.097306
20. Hoseininezhad-Namin MS, Rahimpour E, Aysil Ozkan S, Pargolghasemi P, Jouyban A. Sensing of carbamazepine by AlN and BN nanoclusters in gas and solvent phases: DFT and TD-DFT calculation. J Mol Liq. 2022;353:118750. doi:10.1016/j.molliq.2022.118750
21. Chernozatonskii LA. Carbon nanotube elbow connections and tori. Physics Letters A. 1992;170(1):37-40. doi:10.1016/0375-9601(92)90388-3
22. Apalak MK, Gul K, Arslan YE. Buckling and post-buckling behaviours of adhesively bonded aluminium beams: A review. Rev Adhes Adhes. 2022;10(1):1-46. doi:10.47750/RAA/10.1.01
23. Junejo R, Memon S, Palabiyik IM. Efficient adsorption of heavy metal ions onto diethylamine functionalized calix[4]arene based silica resin. Eurasian Chem Commun. 2020;2(7):785-97. doi:10.33945/SAMI/ECC.2020.7.6
24. Kundu R, Biswas C, Ahmed J, Naime J, Ara MH. A study on the adsorption of cadmium(ii) from aqueous solution onto activated carbon originated from bombax ceiba fruit shell. J Chem Heal Risks. 2020;10(4):243-52. doi:10.22034/jchr.2020.1903764.1154
25. Vessally E, Musavi M, Poor Heravi MR, Engineering C. A density functional theory study of adsorption ethionamide on the surface of the pristine, Si and Ga and Al -doped graphene. Iran J Chem Chem Eng. 2021;40(6):1720-36. doi:10.30492/IJCCE.2022.532176.4794
26. Shamsin Beyranvand H, Mirzaei Ghaleh Ghobadi M, Sarlak H. Experimental study of carbon dioxide absorption in diethyl ethanolamine (DEEA) in the presence of titanium dioxide (TiO2). Prog Chem Biochem Res. 2020;3(1):55-63. doi:10.33945/SAMI/PCBR.2020.1.7
27. Sun X, Wan X, Li G, Yu J, Vahabi V. Amantadine antiparkinsonian drug adsorption on the AlN and BN nanoclusters: A computational study Phys Lett Sect A. 2020;384(5):126128. doi:10.1016/j.physleta.2019.126128
28. Beheshtian J, Tabar MB, Bagheri Z, Peyghan AA. Exohedral and endohedral adsorption of alkaline earth cations in bn nanocluster. J Mol Model. 2013;19(3):1445-50. doi:10.1007/s00894-012-1702-y
29. Wu HS, Cui XY, Xu XH. Structure and stability of boron nitrides: isomer of B32N32. J Mol Struct THEOCHEM. 2005;717(1-3):107-9. doi:10.1016/j.theochem.2004.09.049
30. Hoseininezhad-Namin MS, Pargolghasemi P, Saadi M, Taghartapeh MR, Abdolahi N, Soltani A, et al. Ab

initio study of tepa adsorption on pristine, Al and Si doped carbon and boron nitride nanotubes. J Inorg Organomet Polym Mater. 2020;30(11):4297-310. doi:10.1007/s10904-020-01677-5
31. Samadizadeh M, Peyghan AA, Rastegar SF. Sensing behavior of bn nanosheet toward nitrous oxide: A dft study. Chin Chem Lett. 2015;26(8):1042-5. doi:10.1016/j.cclet.2015.05.048
32. Xia X, Jelski DA, Bowser JR, George TF. Mndo study of boron-nitrogen analogs of buckminsterfullerene. J Am Chem Soc. 1992;114(16):6493-6. doi:10.1021/ja00042a032
33. Kahkhaie SR, Rajabzadeh H, Najafi M, Razavi R, Lariche MJ. Oxidation of methylene via sn-adsorbed boron nitride nanocage (b 30 n 30): DFT investigation. Silicon. 2019;11(2):995-1000. doi:10.1007/s12633-018-9913-1
34. Najafi M. A theoretical investigation of the N2O + SO2 reaction on surfaces of P-doped C60 nanocage and Si-doped B30N30 nanocage. Results Phys. 2017;7:2619-25. doi:10.1016/j.rinp.2017.07.049
35. Niu H, Sun L, Xu Y, Najafi M. Theoretical investigation of oxidation of NO (NO + ½ O2 → NO2) on surfaces of nickel-doped nanocages (Ni–C60 and Ni–B30N30). J Mol Graph Model. 2019;91:140-7. doi:10.1016/j.jmgm.2019.06.010
36. Sinthika S, Kumar EM, Surya VJ, Kawazoe Y, Park N, Iyakutti K, et al. Activation of CO and CO2 on homonuclear boron bonds of fullerene-like BN cages: first principles study. Sci Rep. 2015;5:17460. doi:10.1038/srep17460
37. Yin D, Yang Y, Yang Y, Fang H. A novel fullerene-like B30N30 structure: Stability and electronic property. Carbon. 2016;102:273-8. doi:10.1016/j.carbon.2016.02.063
38. Della Volpe C, Siboni S. From van der waals equation to acid-base theory of surfaces: A chemical-mathematical journey. Rev Adhes Adhes. 2022;10(1):47-97. doi:10.47750/RAA/10.1.02
39. Abdul-Hameed HM. A coated of Ca/Fe layered hydroxide onto a synthesized adsorbent from (banana peels) for removal of cadmium from simulated wastewater. Caspian J Environ Sci. 2021;19(5):825-8. doi:10.22124/cjes.2021.5223
40. Makiabadi B, Zakarianezhad M. Investigation of Adsorption of the Nitrosamine Molecule as a Carcinogen Agent on the AlN Nanotubes: A DFT Study: A DFT study. Chem Methodol. 2020;4(2):191-202. doi:10.33945/SAMI/CHEMM.2020.2.9
41. Pargolghasemi P, Hoseininezhad-Namin MS, Jadid AP. Prediction of Activities of BRAF (V600E) Inhibitors by SW-MLR and GA-MLR Methods. Curr Comput-Aided Drug Des. 2017;13(3):249-61. doi:10.2174/1573409913666170303113812
42. Faramarzi E, Ghiasi R, Abdoli-Senejani M. An attempt for the quantitative DFT-based interpretation of the conformational preference of negative hyperconjugative anomeric effects in trans-2,3- and trans-2,5-dihalo-1,4-dioxanes. Chem Methodol. 2020;4(3):311-23. doi:10.33945/SAMI/CHEMM/2020.3.8
43. Arıoğlu Ç, Tamer Ö, Avcı D, Atalay Y. Optimized geometry, spectroscopic characterization and nonlinear optical properties of carbazole picrate: A density functional theory study. Indian J Phys. 2018;92(12):1613-21. doi:10.1007/s12648-018-1258-5
44. Perdew JP, Wang Y. Accurate and simple analytic representation of the electron-gas correlation energy. Phys Rev B Condens Matter. 1992;45(23):13244-9. doi:10.1103/PhysRevB.45.13244
45. Becke AD. Density-functional thermochemistry. II. The effect of the Perdew–Wang generalized-gradient correlation correction. Chem Phys. 1992;97(12):9173-7. doi:10.1063/1.463343
46. Su K, Wei J, Hu X, Yue H, Lü L, Wang Y, et al. Systematic comparison of geometry optimization on inorganic molecules. Acta Phys Chim Sin. 2000;16(7):650-1.
47. Su K, Wei J, Hu X, Yue H, Lü L, Wang Y, et al. High-level ab initio energy divergences between theoretical optimized and experimental geometries. Acta Phys Chim Sin. 2000;16(8):722-3.
48. Kazemi M, Rad AS. Sulfur mustard gas adsorption on zno fullerene-like nanocage: Quantum chemical calculations. Superlattice Microst. 2017;106:122-8. doi:10.1016/j.spmi.2017.03.046
49. Deng WQ, Xu X, Goddard WA. New alkali doped pillared carbon materials designed to achieve practical reversible hydrogen storage for transportation. Phys Rev Lett. 2004;92(16):166103. doi:10.1103/PhysRevLett.92.166103
50. Behmanesh A, Salimi F, Ebrahimzadeh Rajaei G. Adsorption behavior of letrozole on pure, Ge- and Si-doped C60 fullerenes: a comparative DFT study. Monatsh Chem. 2020;151(1):25-32. doi:10.1007/s00706-019-02524-1
51. Aihara JI. Reduced homo-lumo gap as an index of kinetic stability for polycyclic aromatic hydrocarbons. J Phys Chem A. 1999;103(37):7487-95. doi:10.1021/jp990092i
52. Li J, Lu Y, Ye Q, Cinke M, Han J, Meyyappan M. Carbon nanotube sensors for gas and organic vapor detection. Nano Lett. 2003;3(7):929-33. doi:10.1021/nl034220x